Air–Water Momentum Flux Observations over Shoaling Waves

F. ANCTIL

Département de génie civil, Université Laval, Québec, Québec, Canada

M. A. DONELAN

National Water Research Institute, Canada Centre for Inland Waters, Burlington, Ontario, Canada

(Manuscript received 14 August 1995, in final form 24 January 1996)

ABSTRACT

This paper deals with simultaneous momentum flux observations from four towers placed at different depths along a shore-normal line at the west end of Lake Ontario, Canada. The towers were at nominal depths of 12, 8, 4, and 2 m, in order to study the influence of shoaling waves on the air–water momentum flux, namely the effect of wave steepness and celerity on the aerodynamic roughness of the water surface. Analysis of the data have shown that the momentum fluxes cannot be explained by mean downwind speed alone (U_{10}), in contrast to open ocean experiments in which the wave maturity is generally near full development. Surface roughness (z_0), normalized on wave height (η), was parameterized by both the inverse wave age (U_{10}/c_p) and the root-mean-square wave slope (θ), with excellent correlation in each case ($r^2 = 0.79$). Multiple regression using both the inverse wave age and the root-mean-square slope lead to the best results: $z_0/\eta = 2.26(U_{10}/c_p)^{1.82}\theta^{3.83}$; $R^2 = 0.90$. These findings are presented as further proof, to other recent observations, that surface roughness is dependent on sea state.

1. Introduction

The air–water momentum flux is fundamental to a number of processes such as wave generation, mixed-layer development, and atmosphere and ocean circulation. It is, however, more difficult to measure than its overland counterpart, creating needs for parametric formulations that would allow simple prediction from routinely recorded parameters such as wind velocity, wave properties, air temperature and humidity, and water-surface temperature.

Many open ocean experiments have produced neutral drag coefficients that showed a general increase with mean wind speed, in agreement with Charnock's (1955) proposal (see, for example, Smith 1980 and Large and Pond 1981). Large scatter in the data, however, suggested other simultaneous influences such as surface waves acting as the roughness elements to the air flow. The effect of wave development on the surface roughness was first explored by Kitaigorodskii and Volkov (1965). Since then, several field campaigns have led to the same conclusion: the surface becomes smoother as waves mature from young steep waves to the older and less steep, albeit much higher, waves near full development. Among the more recent examples of such observations are those reported by Donelan (1990), Geernaert et al. (1986), Hsu (1974), and Smith et al. (1992). However, Toba et al. (1990) came to the opposite conclusion, but Donelan et al. (1993) have argued that the results of Toba et al. arise through an inappropriate combination of field and laboratory roughness measurements.

Open ocean data generally correspond to a narrow range of wave maturity near full development, making them unsuitable for exploring the effect of waves on the roughness. Wider ranges of wave development are observed in fetch-limited studies (Donelan 1990) and in cases where the wave celerity is restricted by water depth (Smith et al. 1992). Celerity and steepness are the wave properties most likely to influence the surface roughness. Consequently a field campaign in which these could be altered would be likely to produce some new insight into the question of wave effects on the surface roughness—or at least to confirm or deny existing ideas. In shoaling, waves undergo marked changes in their celerity and steepness and so concomittant observations of the changes in surface roughness provide a natural test bed for these ideas.

The air–water momentum flux is estimated from the covariance of measured velocities at anemometer height (the eddy correlation method)

$$\frac{\tau_s}{\rho} = -\overline{uw} = u_*^2, \qquad (1)$$

Corresponding author address: Dr. M. A. Donelan, National Water Research Institute, Canada Centre for Inland Waters, P.O. Box 5050, Burlington, Ontario L7R 4A6, Canada.

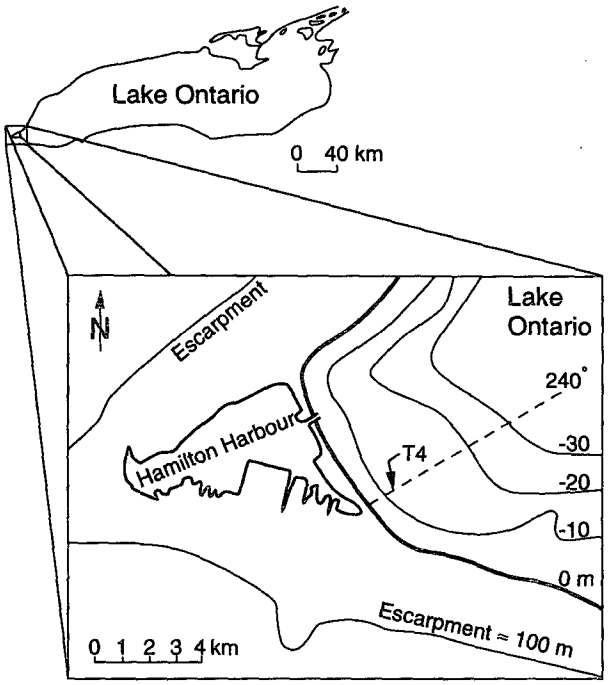

FIG. 1. Location of the experimental site and of the shore-normal line along which the towers were aligned. T4 identifies the location of the main platform (tower 4).

in which τ_s is the surface stress, ρ is the air density, u_* is the friction velocity (defined here), and u and w are the downwind and vertical velocity components with upper- and lowercase denoting means and deviation from the mean, respectively. The overbar denotes a suitable averaging process. The parameterization of the momentum flux, in terms of mean boundary layer measurements, leads to a height-dependent drag coefficient (e.g., Donelan 1990):

$$C_z = \frac{\tau_s}{\rho U_z^2} = \kappa^2 \left[\ln \frac{z}{z_0} - \Psi_u(\zeta) \right]^{-2}, \qquad (2)$$

where κ is von Kármán's constant taken here to be 0.4, z is the measurement height, z_0 is the roughness length, and Ψ is the stability (ζ) dependent profile parameter.

It will be shown in section 3 that suitable corrections to C_z, to compensate for the vertical stress gradient and nonneutral stratification, yield the equivalent neutral drag coefficient value (C_D) for $z = 10$ m. The experimental arrangements are described in section 2, while the observations made are presented in section 4. Finally, discussion and conclusions are reported in sections 5 and 6.

2. Experimental arrangements

The permanent research tower of the Canada Centre for Inland Waters (CCIW) is positioned in about 12 m of water, 1.1 km offshore at the west end of Lake Ontario, near Hamilton. Figure 1 shows a map indicating the location of the research tower, and the local shore-normal line (240°T). For the experiment, three temporary towers were placed at nominal depths of 2, 4, and 8 m, and at distances of 84, 230, and 523 m, respectively, from the beach. The towers were aligned along the normal to the shore, offset by 60 m to the north to avoid possible damage to the signal and power cables from the permanent tower. For simplicity, the four towers will be identified from 1 to 4, starting from the beach and progressing offshore.

Tower 4 was equipped with an array of six wave staffs, which were arranged in a pentagon of 25-cm radius, with one staff in the center. The wave staffs were capacitance gauges of 4.8-mm diameter and were held taut with rubber shock cords. Wind measurements were obtained by a Gill anemometer bivane (height of 12 m), which provides the instantaneous velocity vector in terms of speed and azimuth and elevation angles. Towers 1 to 3 were equipped with triplets of wave staffs, arranged in right isosceles triangles, with two sides of 50 cm and one side of 70.7 cm. The wave staffs were 3.4 m long at tower 1 and 6.6 m long at towers 2 and 3. A Gill anemometer bivane was also used for the wind vector measurements at tower 2, while K-Gill anemometers (Ataktürk and Katsaros 1989) were mounted on towers 1 and 3. The height of the anemometers was 6.2 m for tower 1, 7.8 m for tower 2, and 7.4 m for tower 3. Water and air temperatures were also measured at each tower. All four towers were of the open lattice "Millard" design to minimize flow distortion in both air and water.

Instrument calibrations were performed at CCIW, both before and after field exposure [see Anctil et al. (1994) for a detailed description of the anemometer calibration procedure]. All data from tower 4 were lowpass filtered at 10 Hz and digitized at a sampling rate of 20 Hz. Data from towers 1 to 3 were lowpass filtered at 5 Hz and sampled at 10 Hz. Water temperature measurements from towers 1 to 3 were sampled at 2 Hz.

3. Turbulent flux corrections

The idea of a constant stress layer is based on fairly confining assumptions (Tennekes 1973). It has been shown (e.g., Donelan 1990) that the measured friction velocity (u_*) underestimates the surface value (u_{*s}) by

TABLE 1. General characteristics of selected runs.

Run	Starting time (UTC)	Duration (h)	Wind speed (ms^{-1})	Wind dir.	Waves dir.
166	1613 4 Dec 1987	3.3	7	N	NE
185	1204 15 Dec 1987	5.7	14	E	E

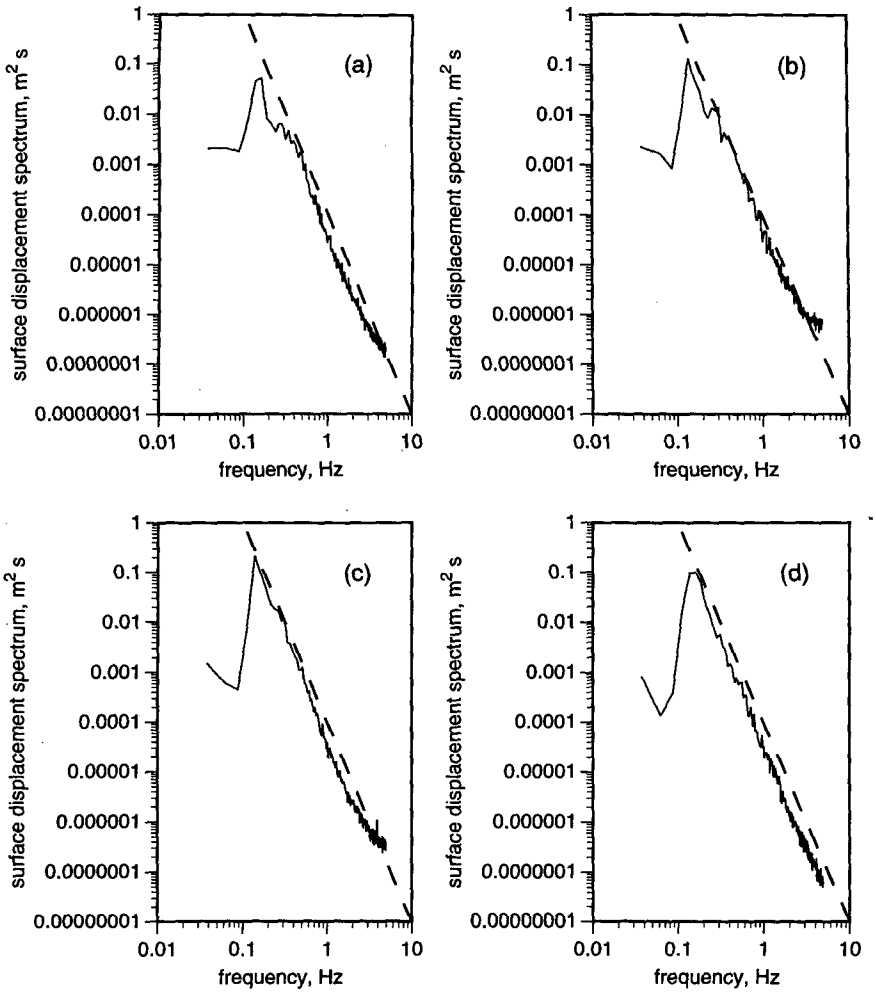

FIG. 2. Surface displacement spectra for run 185, showing f^{-4} reference (dashed): (a) tower 1, (b) tower 2, (c) tower 3, and (d) tower 4.

up to 30% in some cases. This bias can be compensated using

$$u_*^2 = u_{*s}^2\left(1 - \frac{\alpha_0 f_c z}{u_{*s}}\right), \tag{3}$$

in which f_c is the Coriolis parameter [$f_c = 1.454 \times 10^{-4}$ sin(latitude), s^{-1}], and α_0 is the ratio of the geostrophic wind component normal to the surface wind to u_{*s}. Although a large scatter exists, the best estimate for α_0 in neutral conditions is 12 (Clarke 1970).

Here, neutrality is taken to include cases in which the bulk Richardson number R_b is less than 0.01 in magnitude. It is defined by

$$R_b = \frac{gz(T_z - T_s)}{T_z U_z^2}, \tag{4}$$

where T is the potential virtual temperature (K), and the subscripts s and z refer to the surface and the measurement heights, respectively. Even if the effects of buoyancy are small in such cases, they are not negligible. These effects can be accounted for following Monin–Obukhov similarity theory, which relates the mean gradients to a stability ratio, $\zeta = z/L$, where L is known as the Obukhov length. This can also be expressed following Deardoff (1968)

$$\zeta = \kappa C_H C_D^{-3/2} R_b, \tag{5}$$

where C_H is the heat transfer coefficient or Stanton number, taken here to be 0.0012.

When the profile of the mean wind velocity is integrated between the roughness height and the measurement height (Paulson 1970), the diabatic profile influence can be expressed as

$$U_z - U_s = \frac{u_*}{\kappa}\left[\ln\frac{z}{z_0} - \Psi_u(\zeta)\right], \tag{6}$$

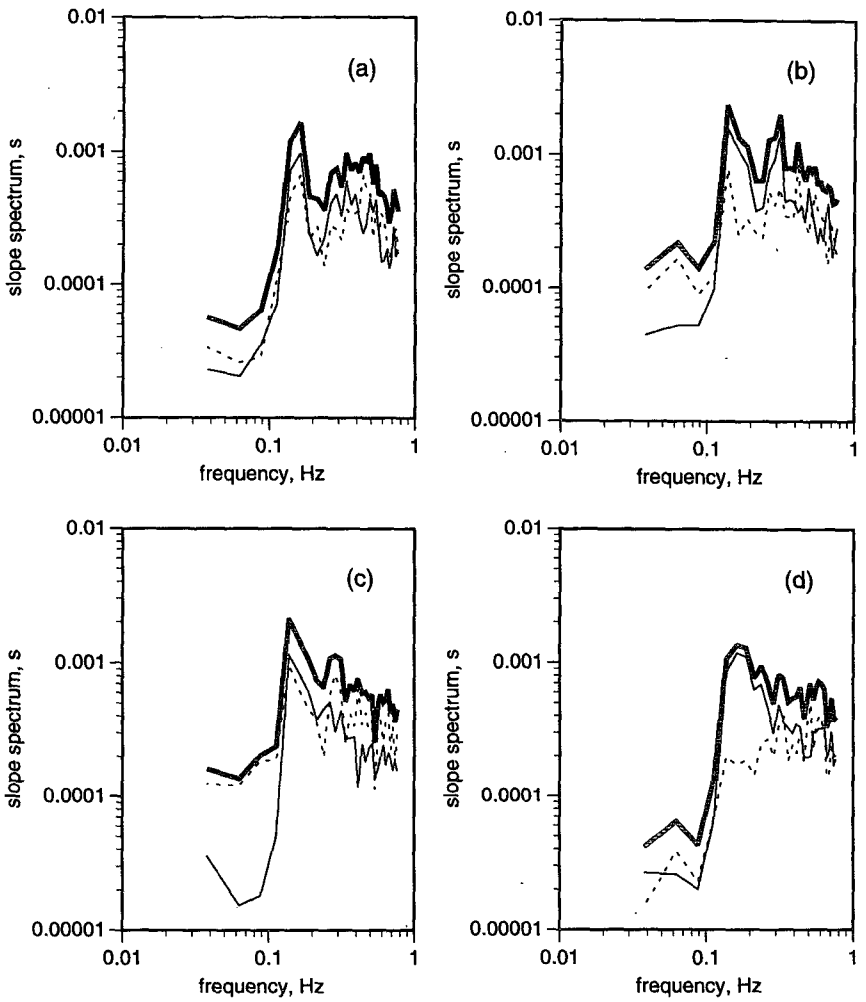

FIG. 3. Slope spectra for run 185, where the total slope is thick solid, x-east is thin solid, and y-north is dashed: (a) tower 1, (b) tower 2, (c) tower 3, and (d) tower 4.

where (Kitaigorodskii and Donelan 1984) for stable conditions, $\zeta > 0$,

$$\Psi_u(\zeta) = -5.4\zeta \tag{7}$$

and for unstable conditions, $\zeta < 0$,

$$\Psi_u(\zeta) = 2\ln\left(\frac{1+X}{2}\right) + \ln\left(\frac{1+X^2}{2}\right) - 2\tan^{-1}X + \frac{\pi}{2} \tag{8}$$

$$X = (1 - 17\zeta)^{1/4}. \tag{9}$$

Using the above formulations, the neutral drag coefficient C_D, for $z = 10$ m, can be deduced from the height-dependent drag coefficient C_z.

4. Results

The dominant wind direction on Lake Ontario is westerly. The towers being located on the west side of the lake, such airflow produces young developing seas, sometimes propagating against preexisting swell. Less frequent northerly and easterly winds produce large waves that shoal between towers 4 and 1 as they approach the beach. Since the aim of this study is to look at the evolution of the surface roughness as the waves shoal, two runs meeting those requirements have been selected. Table 1 summarizes the general characteristics of the selected runs. In run 166, the wind was northerly at about 7 m s^{-1} producing wind waves from the northeast. Run 185 is an easterly storm with winds around 14 m s^{-1} developing large waves from the east. The direction of the waves changes from tower to tower as the waves refract.

Processing of the horizontal and vertical wind velocity, surface displacement, and surface slope signals consisted of applying spectral analysis using fast Fourier transforms (FFTs) based on blocks of 20 min (12 000 points), following the averaging time pro-

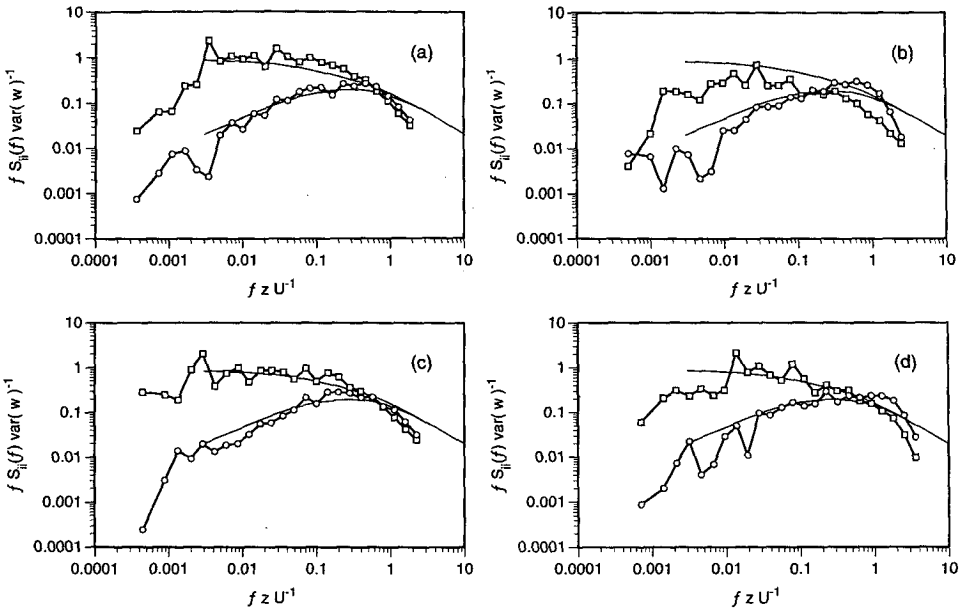

FIG. 4. Normalized downwind (S_{uu} – open square) and vertical wind (S_{ww} – open circle) spectra for run 185, showing respective universal curves from Miyake et al. (1970) in thin lines: (a) tower 1, (b) tower 2, (c) tower 3, and (d) tower 4.

posed by Pierson (1983). To reduce contamination of the low spectral densities through window leakage from the peak, a four-term Blackman–Harris taper (Harris 1978) was applied to the individual blocks. Note that since the sampling rate of the tower 4 signals was twice that of the other towers (20 Hz instead of 10 Hz), all signals from tower 4 were lowpass filtered (using FFT truncation) at 5 Hz, then subsampled to 10 Hz. Corrections to the measured flux variables were performed as described in section 3, to account for the stress gradient and nonneutral measurements and to obtain equivalent observations for $z = 10$ m—the ane-

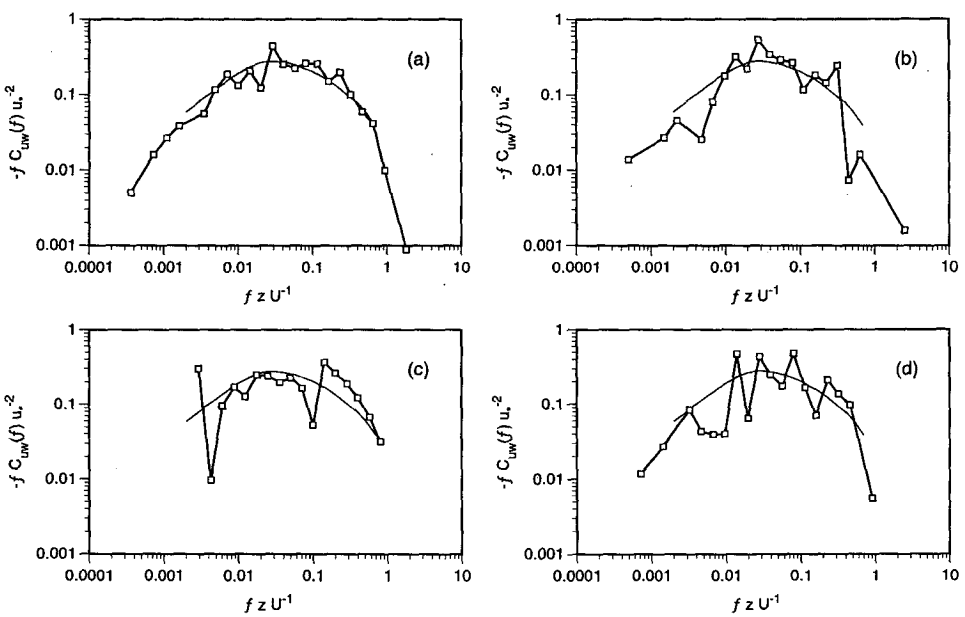

FIG. 5. Normalized uw cospectra (C_{uw} – open square) for run 185, showing the universal curve from Miyake et al. (1970): (a) tower 1, (b) tower 2, (c) tower 3, and (d) tower 4.

TABLE 2a. Wave parameters for run 166.

Block-tower	Depth (m)	η (m)	T_p (s)	c_p (m s^{-1})	θ	Skewness
1-T1	2.9	0.199	5.7	5.01	0.099	0.60
1-T2	4.9	0.219	6.0	6.31	0.098	0.34
1-T3	8.4	0.235	5.3	7.25	0.106	0.03
1-T4	12.4	0.224	5.5	8.04	0.106	0.18
2-T1	2.9	0.178	6.1	5.06	0.095	0.45
2-T2	4.9	0.199	5.3	6.11	0.094	0.27
2-T3	8.4	0.216	5.2	7.18	0.105	0.03

mometer heights were, from tower 1 to 4, 6.2, 7.8, 7.4, and 12 m. Finally, since 20-min averages are quite inaccurate [from Sreenivasan et al. (1978) their expected error is 16% when $U = 10$ m s^{-1} and $z = 10$ m] nonoverlapping groups of four consecutive 20-min averages were pooled to yield 80-min averages, thereby cutting the expected error in half. Because of occasional dropout in the tower signals—note that tower 4 had no dropouts—some 20-min blocks were left out. Group pooling was performed as long as two out of four 20-min blocks were available.

Two orthogonal slope signals (x-east and y-north) were estimated from the wave staff arrays—they were in turn used to produce the root-mean-square slope. Corrections to the slopes were made for the $\sin(x)/x$ response associated with the distance between wave staffs, up to 0.8 Hz. The slope spectra were truncated beyond that frequency.

Only one 20-min block was successfully transmitted to shore by tower 3 during the easterly storm (run 185), which is insufficient to be retained for the discussion, but allows the comparison of simultaneous spectral estimators of the signals from all towers. In Figs. 2 and 3, we show surface displacement and slope (x, y, and total) spectra for each of the four towers. Thirty adjacent spectral estimates are averaged here so that each plotted point has 60 degrees of freedom corresponding to 90% confidence levels of 0.74 and 1.34. Note the increase of energy in the surface displacement spectra for harmonics of the peak frequency as waves shoal, and that the spectra above the peak conform to an f^{-4} power law (Donelan et al. 1985).

The horizontal downwind and vertical wind spectra (S_{uu} and S_{ww}) and cross-spectra (C_{uw}) for each tower are described in Figs. 4 and 5. The number of adjacent estimates averaged increases logarithmically with increasing frequency. The spectra, normalized by the variance of the vertical velocity component, are shown in "natural coordinates" following the work of Miyake et al. (1970). The thin lines represent universal curves obtained by fitting smooth shapes to the data of Miyake et al. (1970). Towers 1 and 3 were equipped with K-Gill anemometers, while Gill anemometer bivanes were used for towers 2 and 4. Figure 4 shows the excellent precision of K-Gill anemometers. However, the anemometer bivane vertical wind variance is overestimated at the high frequency end of the spectrum, much less so at tower 4 than at tower 2. This problem is associated with the second-order response of the vane and, consequently, does not greatly influence the downwind velocity component. On the other hand, all cospectra fit the universal curve well (Fig. 5). The anemometer bivane cospectra are hardly affected by the (above noted) high-frequency imprecision of the vertical velocity, since their energy peaks at much lower frequencies.

The 80-min averages of the main parameters calculated here are given in Tables 2 and 3. Tables 2a and 2b present the sea state parameters for runs 166 and 185, respectively; namely, the water depth, the root-mean-square surface displacement η (the significant wave height is generally given as 4η), the spectral peak period T_p, the spectral peak celerity c_p, the root-mean-square surface slope θ, and the surface displacement skewness. Tables 3a and 3b give the air–sea flux parameters for runs 166 and 185, respectively. The measured flux parameters are given along with the corrected ones for comparison; C_D differs from C_z by as much as 17% and 11% for run 166 and 185, respectively.

5. Discussion

In Fig. 6, the data gathered in this experiment (Tables 2 and 3) are compared with conventional formulas—the solid line represents smooth flows, while the dotted line is Charnock's formula for rough flows and "mature" sea states. One can see that wind speed alone is insufficient to parameterize the large range of C_D measured here (see Donelan 1990 for a different dataset). The group of points on the right side of Fig. 6 belongs to the easterly shoaling storm (run 185). Drag coefficients at towers 1 and 2 are respectively about 40% and 80% larger than values predicted by Charnock's formula. The other group of points corresponds to run 166. In this case, the waves are mature and agreement with Charnock's predictions is close.

TABLE 2b. Wave parameters for run 185.

Block-tower	Depth (m)	η (m)	T_p (s)	c_p (m s^{-1})	θ	Skewness
1-T1	3.2	0.347	5.6	5.25	0.135	0.86
1-T2	5.2	0.405	5.7	6.38	0.142	0.68
1-T4	12.6	0.445	5.6	8.14	0.135	0.26
2-T1	3.2	0.396	6.2	5.32	0.136	0.83
2-T2	5.2	0.527	6.2	6.50	0.152	0.90
2-T4	12.6	0.575	6.2	8.65	0.138	0.24
3-T1	3.3	0.407	7.3	5.41	0.138	0.88
3-T2	5.3	0.575	7.3	6.68	0.162	0.97
3-T4	12.6	0.600	7.4	9.39	0.136	0.23
4-T1	3.3	0.410	7.6	5.42	0.137	0.97
4-T4	12.6	0.643	7.9	9.59	0.137	0.26

TABLE 3a. Air–sea flux parameters for run 166.

Block-tower	U_z (m s^{-1})	$C_z \times 10^3$	R_b	U_{10} (m s^{-1})	$u_{*}s$ (m s^{-1})	$z_0 \times 10^3$ m	$C_D \times 10^3$
1-T1	6.61	1.329	−0.020	7.18	0.242	0.070	1.135
1-T2	7.03	1.346	−0.020	7.49	0.261	0.105	1.216
1-T3	7.05	1.292	−0.023	7.58	0.257	0.075	1.150
1-T4	6.99	1.140	−0.031	7.29	0.246	0.073	1.144
2-T1	5.90	1.373	−0.023	6.44	0.224	0.101	1.209
2-T2	6.03	1.237	−0.030	6.50	0.217	0.061	1.109
2-T3	6.60	1.405	−0.025	7.10	0.256	0.151	1.298

The main parameters computed here are regrouped in Fig. 7. Points of similar runs and block are joined to compare their evolution as the airflow and waves progress toward shore (for sake of clarity, the fourth block of run 185 is not presented). For both runs, the celerity and the surface displacement decrease as waves shoal, while the surface skewness increases. The drag coefficients of run 166 (open squares) are quite uniform throughout. The wind speed is low and the small waves are not greatly influenced in amplitude by shoaling: the surface displacement and the surface slope decrease only slightly as they progress toward shore. The measured parameters of run 185 (filled circles) behave differently. The wind speed is much larger, which produces larger surface displacement and slope. As the waves shoal between towers 4 and 2, the surface slope increases significantly, while the surface displacement decreases slightly. Then follows a zone of active breaking; the measured surface displacement and slope being much lower at tower 1. Note that in run 185, the wind speed is lower at tower 2, probably because of the increased roughness. Indeed, it is interesting that the drag coefficient and wind speed are negatively correlated in this case when the surface waves are undergoing substantial adjustments.

Following the work of Donelan (1990), the relation between the aerodynamic roughness of the water surface and the wave celerity is first examined via correlation between nondimensional variables: z_0/η on the one hand, and U_{10}/c_p (the inverse wave age) on the other hand. Figure 8 shows the relation between both parameters, for run 166 and 185. It can be seen that the inverse wave age varies from values around 1 (mature sea of run 166) to values between 2 and 3 (forced waves of run 185). The regression leads to

$$\frac{z_0}{\eta} = A_0\left(\frac{U_{10}}{c_p}\right)^{B_0}, \qquad (10)$$

where $A_0 = 3.70 \times 10^{-4}$ and $B_0 = 3.22$; ($r^2 = 0.79$), which are close to the values obtained by Donelan (1990), $A_0 = 5.53 \times 10^{-4}$ and $B_0 = 2.66$; ($r^2 = 0.83$), for nonshoaling field data gathered at what is called here tower 4. Donelan's relation is given by the dashed line in Fig. 8. Recent results from the HEXOS experiment off the Dutch coast (Smith et al. 1992) are also in reasonable agreement with (10). It thus seems that the relation between nondimensional roughness length and nondimensional wave celerity proposed by Donelan (1990) holds for shoaling wave conditions.

A similar type of relation is examined between the nondimensional surface roughness and the root-mean-square slope, θ (Fig. 9):

$$\frac{z_0}{\eta} = 2.55 \times 10^3\theta^{6.76}, \quad r^2 = 0.79. \qquad (11)$$

TABLE 3b. Air–sea flux parameters for run 185.

Block-tower	U_z (m s^{-1})	$C_z \times 10^3$	R_b	U_{10} (m s^{-1})	$u_{*}s$ (m s^{-1})	$z_0 \times 10^3$ m	$C_D \times 10^3$
1-T1	13.25	2.587	−0.004	14.25	0.688	2.508	2.328
1-T2	13.43	3.000	−0.005	14.07	0.750	5.524	2.843
1-T4	14.41	2.147	−0.007	14.33	0.683	2.268	2.272
2-T1	14.10	2.482	−0.003	15.12	0.717	2.165	2.247
2-T2	14.32	3.145	−0.004	14.99	0.818	6.567	2.979
2-T4	15.35	1.820	−0.007	15.31	0.671	1.081	1.918
3-T1	12.80	2.340	−0.004	13.76	0.632	1.644	2.107
3-T2	12.37	2.663	−0.005	12.96	0.651	3.464	2.520
3-T4	14.09	1.760	−0.008	14.09	0.606	0.908	1.847
4-T1	12.21	2.435	−0.004	13.14	0.615	1.955	2.194
4-T4	13.49	1.773	−0.008	13.49	0.583	0.962	1.870

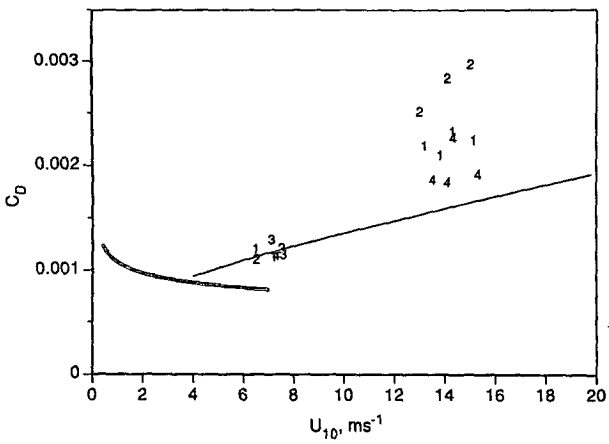

FIG. 6. Drag coefficient observations as a function of mean wind speed. The figures correspond to the tower numbers; the thick and thin lines give the smooth flow condition, $z_0 u_*/\nu = 0.11$, and Charnock's relation for rough flow, respectively.

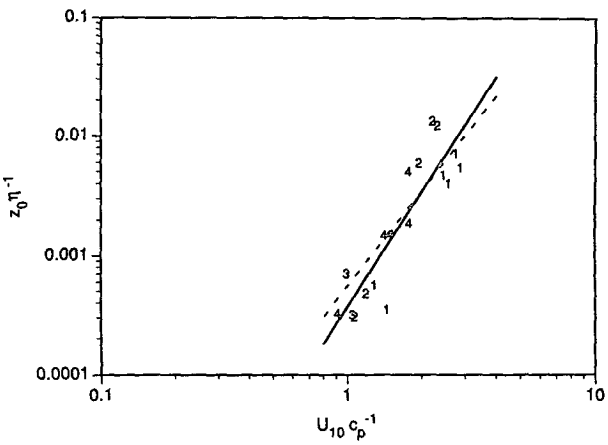

FIG. 8. Nondimensional roughness as a function of inverse wave age. The figures correspond to the tower numbers, the solid line is (10), and the dashed line is from Donelan (1990).

Since this correlation is as conclusive as the one with the inverse wave age, multiple correlation is considered next.

The correlation coefficient (r^2) is a good indicator of the quality of a simple regression, but it does not exist for multiple regression. In such cases, one may instead compute the multiple regression coefficient (R^2), which has a slightly different meaning. It gives an estimate of how well all regressors fit the data (e.g., Wonnacott and Wonnacott 1981):

$$R^2 = \frac{[\sum_{i=1}^{N} (\hat{y}_i - \bar{y})^2]}{[\sum_{i=1}^{N} (y_i - \bar{y})^2]}, \qquad (12)$$

where y_i are the parameterized data, $\hat{y}_i$ are the results of the regression formulation, and the overbar denotes an average process. In short, it is the ratio of the variation of y explained by all parameters, to the total variation of y. For a single regressor, $R^2 = r^2$.

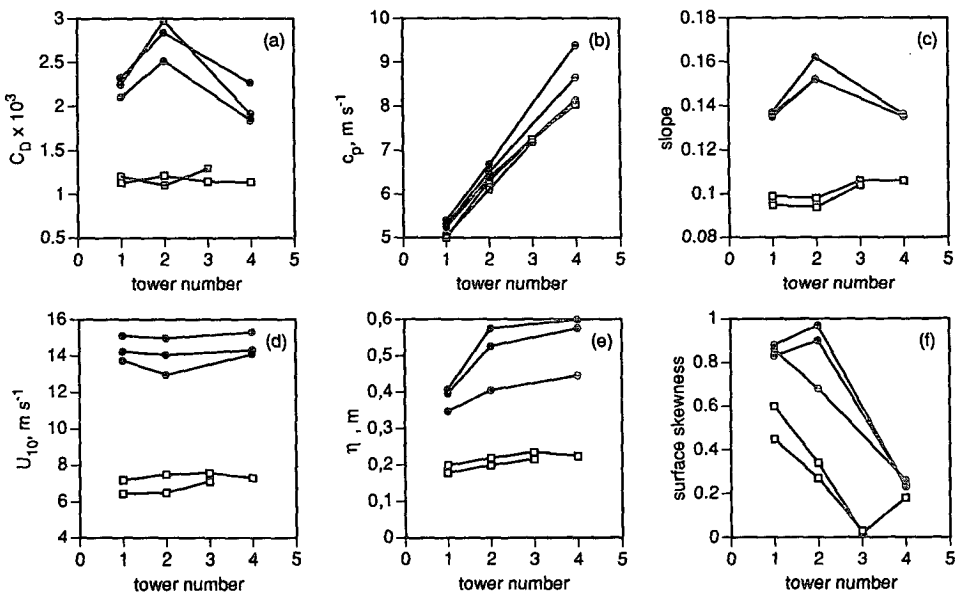

FIG. 7. Plots showing the spatial evolution of measured parameters for run 166 (open square) and run 185 (filled circle): (a) is drag coefficient, (b) is spectral peak celerity, (c) is root-mean-square surface slope, (d) is mean wind speed, (e) is root-mean-square surface displacement, and (f) is surface skewness.

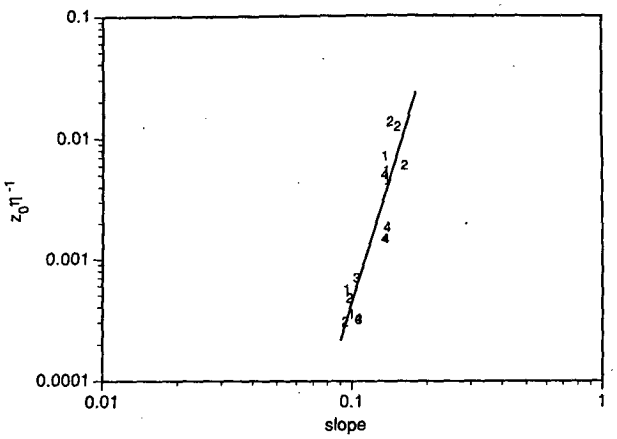

FIG. 9. Nondimensional roughness as a function of root-mean-square slope. The figures correspond to the tower numbers, and the solid line is (11).

Multiple regression yields

$$\frac{z_0}{\eta} = 2.26\left(\frac{U_{10}}{c_p}\right)^{1.82}\theta^{3.83}, \quad R^2 = 0.90, \qquad (13)$$

which is an improvement on both (11) and (12). It does seem that both inverse wave age and root-mean-square slope do influence the variation of nondimensional roughness.

6. Conclusions

Field measurements were conducted simultaneously at four towers located at nominal depths of 2, 4, 8, and 12 m, along a shore-normal line. They have provided data, with both airflow and waves progressing toward shore, allowing the measurement of air–sea fluxes as waves shoal.

These data allowed the examination of the effect of the waves on the surface aerodynamic roughness as the former were being modified by the diminishing depth. Previous attempts to relate surface roughness to sea state have been derived from data taken (usually) at a single site under a variety of conditions obtained over long periods. These shoaling data provide a unique opportunity to hold the external atmospheric conditions essentially constant (for two distinct cases) while observing the changes in surface stress brought about by the spatial variation of wave properties.

We find that the resulting neutral drag coefficients are not well represented by a simple wind dependence, such as that suggested by many open ocean experiments and most succinctly embodied in the relation due to Charnock (1955). On the other hand, the ratio of roughness length to wave height is well correlated with the inverse wave age, in good agreement with the results of Donelan (1990) for fetch-limited waves. Root-mean-square slope also has a strong influence on the roughness length, giving further evidence that the wave field affects the air–water momentum flux. In fact, the best correlation is obtained using both the inverse wave age and the root-mean-square slope.

It would seem that the aerodynamic roughness of pure wind seas may be adequately parameterized by the wave height, age and slope. However, it is clear that such simple relationships may not be adequate in confused seas and should therefore be used with care.

Acknowledgments. The experiment was supported in part by the Panel for Energy Research and Development under study 62124, task 6.2. We thank M. Skafel for comments and criticisms of the manuscript. We acknowledge with gratitude the help of K. Kahma, who designed the K-Gill calibration apparatus, and the following members of the staff of NWRI: S. Beal, D. Beesley, J. Cooper, Y. Desjardins, R. Desrosiers, J. Dolanski, T. Nudds, M. Pedrosa, L. Peer, F. Roy, H. Savile, M. Skafel, I. Tsanis, and J. Valdmanis.

REFERENCES

Anctil, F., M. A. Donelan, W. M. Drennan, and H. C. Graber, 1994: Eddy correlation measurements of air–sea fluxes from a discus buoy. *J. Atmos. Oceanic Technol.*, **11,** 1144–1150.

Ataktürk, S. S., and K. B. Katsaros, 1989: The K-Gill: A twin propeller-vane anemometer for measurements of atmospheric turbulence. *J. Atmos. Oceanic Technol.*, **6,** 509–515.

Charnock, H., 1955: Wind stress over a water surface. *Quart. J. Roy. Meteor. Soc.*, **81,** 639–640.

Clarke, R. H., 1970: Observational studies of the atmospheric boundary layer. *Quart. J. Roy. Meteor. Soc.*, **96,** 91–114.

Deardoff, J. W., 1968: Dependence of air–sea transfer coefficients on bulk stability. *J. Geophys. Res.*, **73**(8), 2549–2557.

Donelan, M. A., 1990: Air–sea interaction. *The Sea,* Vol. 9, B. LeMéhauté and D. M. Hanes, Eds., Wiley, 239–292.

——, J. Hamilton, and W. H. Hui, 1985: Directional spectra of wind-generated waves. *Philos. Trans. Roy. Soc. London,* **A315,** 509–562.

——, F. W. Dobson, S. D. Smith, and R. J. Anderson, 1993: On the dependence of sea surface roughness on wave development. *J. Phys. Oceanogr.,* **23,** 2143–2149.

Geernaert, G. L., K. B. Katsaros, and K. Ritcher, 1986: Variation of the drag coefficient and its dependence on sea state. *J. Geophys. Res.*, **91**(C6), 7667–7679.

Harris, F. J., 1978: On the use of windows for harmonic analysis with the discrete Fourier transform. *Proc. IEEE,* **66,** 51–83.

Hsu, S. A., 1974: A dynamic roughness equation and its application to wind stress determination at the air–sea interface. *J. Phys. Oceanogr.,* **4,** 116–120.

Kitaigorodskii, S. A., and Y. A. Volkov, 1965: On the roughness parameter of the sea surface and the calculation of momentum flux in the near-water layer of the atmosphere. *Izv. Atmos. Oceanic Phys.,* **1,** 973–988.

——, and M. A. Donelan, 1984: Wind–wave effects on gas transfer. *Gas Transfer at Air–Water Surface,* Reidel, 147–170.

Large, W. G., and S. Pond, 1981: Open ocean momentum flux measurements in moderate to strong winds. *J. Phys. Oceanogr.,* **11,** 324–336.

Miyake, M., R. W. Stewart, and R. W. Burling, 1970: Spectra and cospectra of turbulence over water. *Quart. J. Roy. Meteor. Soc.,* **96,** 138–143.

Paulson, C. A., 1970: The mathematical representation of wind speed and temperature profiles in unstable atmospheric surface layer. *J. Appl. Meteor.*, **9,** 857–861.

Pierson, W. J., 1983: The measurement of the synoptic scale wind over the ocean. *J. Geophys. Res.*, **88**(C3), 1683–1708.

Smith, S. D., 1980: Wind stress and heat flux over the ocean at gale force winds. *J. Phys. Oceanogr.*, **10,** 706–726.

——, R. J. Anderson, W. A. Oost, C. Kraan, N. Maat, J. DeCosmo, B. Katsaros, K. L. Davidson, K. Bumke, L. Hasse, and H. M. Chadwick, 1992: Sea surface wind stress and drag coefficients: The HEXOS results. *Bound.-Layer Meteor.*, **60,** 109–142.

Sreenivasan, K. R., A. J. Chambers, and R. A. Antonia, 1978: Accuracy of moments of velocity and scalar fluctuations in the atmospheric surface layer. *Bound.-Layer Meteor.*, **14,** 341–359.

Tennekes, H., 1973: The logarithmic wind profile. *J. Atmos. Sci.*, **30,** 234–238.

Toba, Y., N. Iida, H. Kawamura, N. Ebuchi, and I. S. F. Jones, 1990: Wave dependence of sea-surface wind stress. *J. Phys. Oceanogr.*, **20,** 705–721.

Wonnacott, T. H., and R. J. Wonnacott, 1981: *Regression: A Second Course in Statistics.* John Wiley & Sons, 556 pp.